Letter

Proposal for realization and detection of Kitaev quantum spin liquid with Rydberg atoms

Yi-Hong Chen,[1,2,*] Bao-Zong Wang,[1,2,*] Ting-Fung Jeffrey Poon,[1,2] Xin-Chi Zhou,[1,2] Zheng-Xin Liu,[3] and Xiong-Jun Liu[1,2,4,5,†]

[1]*International Center for Quantum Materials, School of Physics, Peking University, Beijing 100871, China*

[2]*Hefei National Laboratory, Hefei 230088, China*

[3]*Department of Physics, Renmin University of China, Beijing 100872, China*

[4]*International Quantum Academy, Shenzhen 518048, China*

[5]*CAS Center for Excellence in Topological Quantum Computation, University of Chinese Academy of Sciences, Beijing 100190, China*

(Received 12 November 2023; revised 29 July 2024; accepted 3 October 2024; published 2 December 2024)

The Kitaev chiral spin liquid has captured widespread interest in recent decades because of its intrinsic non-Abelian excitations, yet the experimental realization is challenging. Here we propose to realize and detect Kitaev chiral spin liquid in a deformed honeycomb array of Rydberg atoms. With a laser-assisted dipole-dipole interaction mechanism which realizes both effective hopping and pairing terms for hard-core bosons, together with van der Waals interactions, we achieve the pure Kitaev model with high precision. The gapped non-Abelian spin liquid phase is then obtained under experimental conditions. Moreover, we propose innovative strategies to probe the chiral Majorana edge modes by light Bragg scattering and by imagining their chiral motion. Our proposed scheme broadens the range of quantum spin models with exotic topological phases that can be realized and detected in atomic systems, and makes an important step toward manipulating non-Abelian anyons.

DOI: 10.1103/PhysRevResearch.6.L042054

Introduction. Topological order is a captivating concept in condensed matter physics that goes beyond Landau paradigm and can host exotic quasiparticle excitations as anyons [1]. The Kitaev model on the honeycomb lattice with an exactly solvable ground state is an ideal platform to prepare for gapped quantum spin liquid (QSL) phases with the Ising-type non-Abelian topological order [2]. The braiding of the Ising-type anyonic excitations results in non-Abelian Berry phase within the space of topologically degenerate states, which remains robust against local perturbations [3–7]. Furthermore, the promotion of braiding operations to unitary gates is the key of the promising fault-tolerant topological quantum computation [3,8–10]. Significant efforts have been made in solid-state systems [11–19], but the confirmation of the Kitaev QSL phases is still ongoing [20–26].

Alternatively, quantum simulation [27–29] may provide a route to achieve a clean and highly controllable realization of the Kitaev spin liquid. The dynamical simulation approaches were recently proposed based on the earlier schemes of Floquet spin liquid [30,31], including a digital simulation through Rydberg atoms [32] and a dynamical simulation [33] on the optical lattice. The Rydberg atom platform is particularly suitable for simulating the spin models [34–41], with Rydberg atoms in optical tweezer arrays [42–46] resembling lattice spins, and the dipole-dipole and van der Waals (vdW) interactions inherently produce XY and Ising interactions [34,47]. This capability of simulating quantum spin systems has been verified in numerous experiments, including quantum Ising model [48–53], XY model [54,55], one-dimensional bosonic symmetry-protected topological phase [56], and abelian quantum spin liquid [57]. Nevertheless, the simulation of generic spin interactions could be challenging. To this end, the laser-assisted dipole-dipole interaction (LADDI) technique in Rydberg atom array is introduced in our recent works [58–60], extending Raman-engineered single-particle couplings studied in optical lattices [61–69]. This technique provides a flexible tool to precisely control spin-exchange interactions through lights, equipping us with the capability to realize more intricate and exotic quantum spin models.

In this Letter, we propose an innovative scheme to precisely realize and probe the Kitaev spin liquid phase in a deformed honeycomb array of Rydberg atoms. The Kitaev exchange interactions are decomposed into the hopping and pairing terms of the hard-core bosons, which are realized based on a fundamentally new type of LADDI proposed here. Together with vdW interaction, we show the Kitaev spin liquid model can be realized with a high tunability and precision. We further propose the feasible schemes to detect the non-Abelian spin liquid, including the bulk gap and chiral edge state, through dynamical response and unidirectional transport measurements. Our work opens a promising avenue for exploring the quantum spin liquids and their potential applications.

Model. The paradigmatic Kitaev model is an ideal platform to prepare for non-Abelian anyonic excitations. The model under consideration is defined by a spin-1/2 system on a

*These authors contributed equally to this work.

†Contact author: xiongjunliu@pku.edu.cn

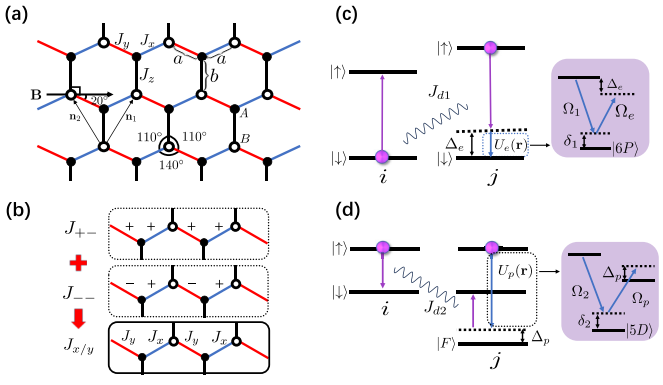

FIG. 1. Sketch of the model and realization. (a) The transformed lattice configuration of the Kitaev honeycomb model, which is realized by Rydberg atoms trapped in the optical tweezers. The angle between bonds and bond lengths deviates slightly from the ideal honeycomb lattice. (b) The alternating J_x, J_y configuration consists of a uniform hopping term J_{+-} and a staggered pairing term J_{--} with the same absolute value. (c), (d) Illustration of LADDIs. Inset: the two-photon Raman processes (see details in the Supplemental Material). (c) The hopping process J_{+-}, where Raman potential $U_e = \Omega_1^\star \Omega_e/\delta_1$ compensates the energy offset, with δ_1 representing the detuning of the two Raman lasers to the intermediate state. (d) The pairing interaction J_{--}, driven by the Raman potential $U_p = \Omega_2^\star \Omega_p/\delta_2$, causes the same spin flip process on both sites.

honeycomb array, as depicted in Fig. 1(a), and described by the Hamiltonian given by

$$H = -\sum_{\langle ij\rangle_\gamma} J_\gamma s_i^\gamma s_j^\gamma - \sum_{j,\gamma} h_\gamma s_j^\gamma,\ \gamma = x, y, z. \tag{1}$$

Here $\langle ij\rangle_\gamma$ labels $\gamma(= x, y, z)$ type, the summation takes over all the bonds on the honeycomb lattice, and J_γ denotes the Ising coupling strength for spin components $s_{i(j)}^\gamma$ of the γ-bond connecting sites $\mathbf{r}_i$ and $\mathbf{r}_j$ [Fig. 1(a)]. The ground states of the exactly solvable model at $h_\gamma = 0$ include three gapped A phases and one gapless B phase featured by Majorana fermions in the Z_2 gauge field [2]. Applying the Zeeman field breaks time reversal symmetry and drives B phase into a non-Abelian spin liquid.

Nonetheless, directly simulating these bond-dependent Ising interactions with the Rydberg atom array is out of reach, since the intrinsic dipole-dipole and vdW interactions between Rydberg atoms are of the XXZ type [34,47]. To facilitate the description of our key idea, we decompose these Ising interactions into hopping (J_{+-}) and pairing (J_{--}) terms in the hard-core boson language [70]

$$\begin{aligned}\sum_{\langle ij\rangle_x} J_x s_i^x s_j^x &= \textstyle\sum_{\langle ij\rangle_x} (J_{+-}^x b_i^\dagger b_j + J_{--}^x b_i b_j) + \text{H.c.},\\ \sum_{\langle ij\rangle_y} J_y s_i^y s_j^y &= \textstyle\sum_{\langle ij\rangle_y} (J_{+-}^y b_i^\dagger b_j + J_{--}^y b_i b_j) + \text{H.c.},\end{aligned} \tag{2}$$

which shall be realized separately. Here the hard-core bosons are defined as $b_j = s_j^-$ with $b_j^2 = 0$, the hopping and pairing terms along (x, y) bonds are the same (opposite) for x (y) bonds, namely, $J_{+-}^x = J_{--}^x = J_x/4$ and $J_{+-}^y = -J_{--}^y = J_y/4$ [see Fig. 1(b)]. Unlike the hopping term arising from dipole-dipole interaction, the pairing term is intrinsically not present for Rydberg atoms. We present here an original scheme to solve the challenge and realize both the hopping and pairing terms through a type of LADDI. Together with a well engineered vdW interaction to realize the z-bond interaction, we achieve the model (1) with high precision.

Experimental scheme. We demonstrate the realization of controllable hopping and pairing terms in a 2D Rydberg atom array, composed of ^{87}Rb atoms trapped in an optical tweezer array with the deformed honeycomb lattice configuration. For our purpose, the bond angles of the array are deformed to 110°, and the x, y (z) bond lengths are a (b) [Fig. 1(a)]. A real in-plane magnetic field is introduced to define the "quantization axis" perpendicular to the z bond and at an angle $\theta = 20°$ to the x, y bond. The spin states are represented by Rydberg states $|\downarrow\rangle = |n_D D_{\frac{5}{2}}, m_J = \frac{5}{2}\rangle$ and $|\uparrow\rangle = |n_P P_{\frac{3}{2}}, m_J = \frac{3}{2}\rangle$.

The hopping term J_{+-}, which transforms $|\downarrow\rangle_i|\uparrow\rangle_j$ into $|\uparrow\rangle_i|\downarrow\rangle_j$, can be constructed through a laser-assisted process, here i and j label two nearest neighbor sites on the x or y bonds. As shown in Fig. 1(c), the bare dipole-dipole interaction J_{d1} which couples $|\downarrow\rangle_i|\uparrow\rangle_j \to |\uparrow\rangle_i|\downarrow\rangle_j$ is suppressed by a detuning $\Delta_e = (E_\uparrow - E_\downarrow)_j - (E_\uparrow - E_\downarrow)_i$. The detuning is induced by introducing a site-dependent energy shift to the spin-up state $E_{\uparrow,i} = E_P + \Delta_i$. In the presence of Raman potential $U_e(\mathbf{r})e^{i\Delta_e t}$, this energy offset is compensated, enabling the laser-assisted exchange process. Therefore, by applying energy offset Δ_e, the exchange couplings are completely controllable by the lasers. From a standard perturbation theory [71], we obtain

$$J_{+-} = \frac{U_e(\mathbf{r}_j)}{\Delta_e} J_{d1} + O((J_{d1}, U_e)^4), \tag{3}$$

The pairing term J_{--} transforms $|\uparrow\rangle_i|\uparrow\rangle_j$ to $|\downarrow\rangle_i|\downarrow\rangle_j$ and can only be driven by laser assistance. We introduce another laser-assisted process through an intermediate state $|F\rangle = |n_F F_{7/2}, m_J = 7/2\rangle$, as illustrated in Fig. 1(d). The dipole-dipole interaction J_{d2}, which couples $|\uparrow\rangle_i|F\rangle_j$ to $|\downarrow\rangle_i|\downarrow\rangle_j$, takes effect when the detuning $\Delta_p = (E_\downarrow - E_\uparrow)_i + (E_\downarrow - E_F)_j$ is compensated by the Raman potential $U_p(\mathbf{r})e^{i(E_\uparrow - E_F - \Delta_p)t}$, giving rise to the process $|\uparrow\rangle_i|\uparrow\rangle_j \to |\uparrow\rangle_i|F\rangle_j \to |\downarrow\rangle_i|\downarrow\rangle_j$. We then obtain from perturbation the pairing coefficient

$$J_{--} = -\frac{U_p(\mathbf{r}_j)}{\Delta_p} J_{d2} + O((J_{d2}, U_p)^4), \tag{4}$$

the resonant Raman coupling regime [71].

The sign configurations of $J_{+-}^{x,y}$ and $J_{--}^{x,y}$ along (x, y) bonds can be feasibly achieved via on-site tuning of the Raman potentials (see details in the Supplemental Material [71]). With the site-dependent energy shift Δ_i (Δ_i') (see [55] for experimental realization of nonuniform energy shift), which has a periodicity of every eight sites [Fig. 2(a)], achievable through local tuning of optical tweezers, we can apply different Raman potential $U_{e,p}$ to different bonds separately by matching the Raman potential frequency with the corresponding detuning $\Delta_{e,p}$ [Fig. 2(b)]. The phases of the Raman potential U_e are chosen to ensure a uniform sign for U_e/Δ_e, resulting in $J_{+-}^x = J_{+-}^y$. Meanwhile, the signs of U_p exhibit a distinct staggered pattern along the row, giving rise to the relation of $J_{--}^x = -J_{--}^y$. This yields the $J_{x,y}$ terms of the Kitaev model, as depicted in Fig. 1(c).

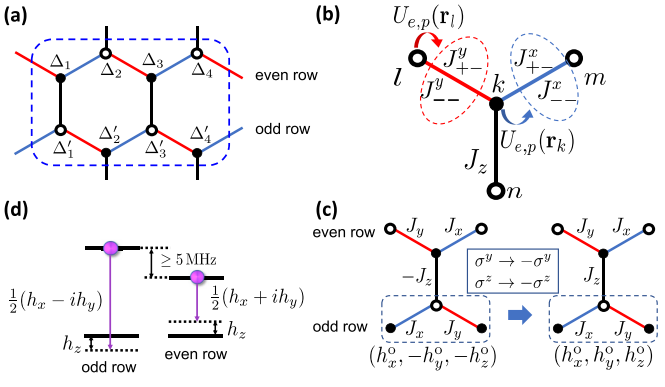

FIG. 2. Detailed configuration of the experimental proposal. (a) The on-site energy shifts, the detunings Δ_i and Δ'_i at even and odd rows are set to be different. (b) The coupling at a bond is determined only by the Raman potential on one side. Raman potentials $U_{e,p}(\mathbf{r}_l)$ $[U_{e,p}(\mathbf{r}_k)]$ have frequencies corresponding to $\Delta_{e,p}$ on the $\langle lk\rangle$ ($\langle km\rangle$) bond. (c) A unitary transformation that transforms $\sigma_{y,z}$ in odd rows to $-\sigma_{y,z}$, resulting in J_z changing sign but $J_{x,y}$ remaining unchanged. It also changes the sign of $h_{y,z}$ in odd rows (labeled $h^o_{y,z}$). (d) The Zeeman terms $h_{y,z}$ are opposite in even and odd rows, which are induced independently by microwaves.

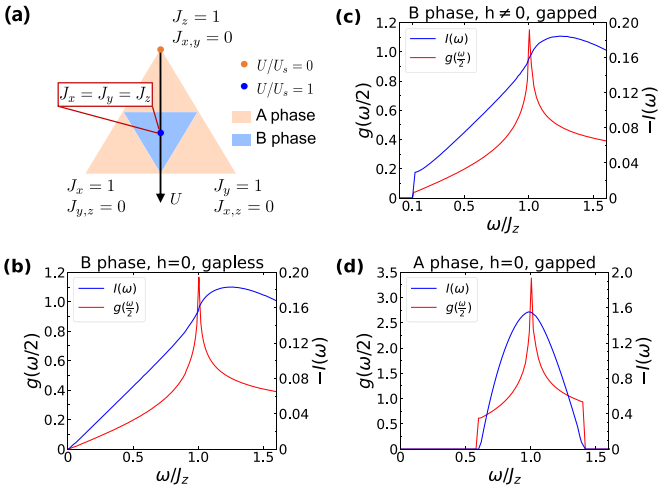

FIG. 3. Phase diagram and detection of the bulk spectra. (a) Ground state phase diagram of the Kitaev honeycomb model. The parameters evolve along the black line by tuning the strength of Raman potential U. (b)–(d) Two-spin response $I(\omega)$ and underlying density of states $g(\omega/2)$. (b)–(c) The Kitaev B phase [2] with the parameters $J_x = J_y = J_z$. The gapless B phase acquires a topological gap for $h_{x,y,z} = 0.5$MHz. (d) The abelian Kitaev A phase at $J_x = J_y = J_z/5$.

The J_z term arises from the intrinsic vdW interaction of Rydberg atoms, characterized by $V_{\sigma\sigma'} \propto n_\sigma n_{\sigma'}$, where n_σ denotes the occupation number at state $|\sigma = \uparrow, \downarrow\rangle$. From $s^z = (n_\uparrow - n_\downarrow)/2$, we obtain the J_z term by

$$H_{\text{inter-row}} = -\sum_{\langle ij\rangle_z} J_z(n_{i,\uparrow} - n_{i,\downarrow})(n_{j,\uparrow} - n_{j,\downarrow})/4. \quad (5)$$

Here $J_z = V_{\downarrow\uparrow} + V_{\uparrow\downarrow} - V_{\downarrow\downarrow} - V_{\uparrow\uparrow}$. Note that the lattice sites on even and odd rows have different energy offsets Δ_i and Δ'_i, respectively [Fig. 2(a)]. Thus, the interactions J_{+-} and J_{--} at z bonds are offresonant and negligible. Only the J_z coupling remains along the z bonds.

Our proposal offers high tunability for simulating the Kitaev spin liquid, encompassing both Kitaev A and B phases [2]. The pure bond-dependent Ising couplings can be precisely achieved and further tuned by Raman potentials $U_{e,p}$, as confirmed from numerical results [71]. Thus, adjusting $U_{e,p}$ adiabatically while keeping J_z to be constant can drive the system from the A phase with the parameters $J_x = J_y = 0$ to the B phase with $J_x = J_y = J_z$, as illustrated by the black line in Fig. 3(a).

The non-Abelian anyons emerge in phase B by applying Zeeman terms $h_{x,y,z}$ to open a topological gap. The naturally realized J_z is typically ferromagnetic ($J_z > 0$). We can physically transform it into antiferromagnetic interactions by properly applying Zeeman terms. First, we map $\sigma_{y,z}$ to $-\sigma_{y,z}$ in odd rows through a unitary transformation [Fig. 2(c)], causing J_z to change sign while leaving $J_{x,y}$ unchanged. This transformation also flips $h_{y,z}$ in odd rows to $-h_{y,z}$. Then, to maintain an effective uniform Zeeman field, the originally applied Zeeman components $h_{y,z}$ should have opposite signs in even and odd rows, which can be implemented as follows.

The h_z term is directly obtained by setting detuning (h^e_z) for the transition induced by Raman potential U_p between $|\downarrow\rangle_i|\downarrow\rangle_j$ and $|\uparrow\rangle_i|\uparrow\rangle_j$. A staggered configuration of h_z is resulted by tuning opposite detunings in even and odd rows [Fig. 2(d)]. The $h_{x,y}$ terms are induced by microwaves that drive spin-flip transitions. Similarly, the h_y terms on odd and even rows can be controlled independently by microwaves with different frequencies, hence a staggered configuration of h_y can be feasibly achieved by tuning the coupling phases [Fig. 2(d)]. More details are presented in the Supplemental Material [71].

Numerics. We take $n_P = 44$, $n_D = 42$, and $n_F = 40$ to exemplify the high precision and feasibility of the realization [71]. On (x, y) bonds we have $J_{x,y} \simeq -4$ MHz for $a = 4.7\,\mu$m. By choosing the quantization axis and lattice geometry shown in Fig. 1(a), we find that on the z bond one can set $J_z \simeq 4.0$ MHz for $b = 4.2\,\mu$m, while on the x, y bonds it is quite small $|J_z| < 0.16$ MHz, giving a nearly pure Kitaev model. Further, we have verified that the longer-range couplings are all less than 5.2% of the nearest-neighboring terms, hence being negligible. Finally, numerical study has shown that applying the Zeeman term leads to a topological gap in the B phase that $E_{\text{gap}} \approx 0.1J_z = 0.4$ MHz for $h_{x,y,z} = 0.5$ MHz [72]. Such interactions are sufficiently large for Rydberg atom lifetime $\tau \gtrsim 60\,\mu\text{s} = 240|J_{x,y,z}|^{-1}$ at temperature $T = 77$ K in the experiment [36,71,73].

Detection of the bulk spectrum. We now turn to the detection of the bulk spectra of Majorana fermions c_i [2]. The gap is detected through a minimal perturbation approach utilizing $c_i c_{j\,\langle ij\rangle_\gamma}$ to excite the Majorana fermions, equivalent to $s^\gamma_i s^\gamma_{j\,\langle ij\rangle_\gamma}$ in the spin representation. The two-spin perturbation Hamiltonian given by $\Delta H = \sum_{\langle ij\rangle_{\gamma=x,y}} \Delta J s^\gamma_i s^\gamma_j$ is applied shorter than the typical inverse gap ($\sim$2.5 μs) in the B phase with Zeeman field. Experimentally, this is achieved by varying $J_{x,y}$ through Raman potentials. The response is determined by retarded function $iF(t) = \langle[\Delta H(t), \Delta H(0)]\rangle\theta(t)$, where the

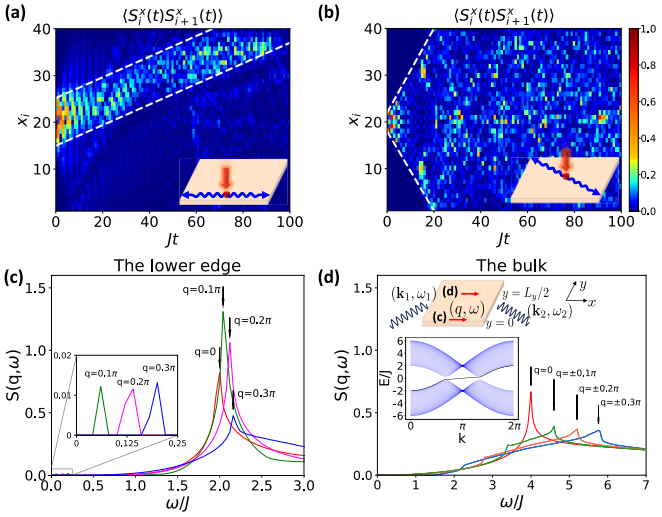

FIG. 4. Identifying the chiral edge modes. (a), (b) Applying a perturbation on an x bond (red point) and then measuring the propagation of spin correlation (blue wavy line) on a 40×40-site system. (a) The perturbation is imposed at the edge. Unidirectional propagation is observed. (b) The perturbation is applied in the bulk, and it rapidly diffuses into the entire system symmetrically. (c), (d) The dynamical structure factor. (c) The $y = 0$ edge region shows peaks at both low and high frequencies at positive transfer momenta. (d) The bulk region only shows peaks in high frequency but symmetric in both positive and negative momenta. Inset: Schematic of light Bragg scattering applied on edge or bulk (red arrow) and energy spectrum with lower edge state (black line).

average is taken over ground state. The Fourier transformation $I(\omega) \equiv \int_0^\infty dt e^{i\omega t} F(t)$ yields [74]

$$I(\omega) = -4\pi \sum_{\mathbf{q}} \delta(\omega - 4|s_{\mathbf{q}}|)(\mathrm{Im}[h_{\mathbf{q}} s_{\mathbf{q}}^*]/|s_{\mathbf{q}}|)^2 \qquad (6)$$

for $\omega > 0$ and $I(-\omega) = -I(\omega)$. Here $s_{\mathbf{q}} = (J_z + J_x e^{i\mathbf{q}\cdot\mathbf{n}_1} + J_y e^{i\mathbf{q}\cdot\mathbf{n}_2})/4$ and $h_{\mathbf{q}} = \Delta J(e^{i\mathbf{q}\cdot\mathbf{n}_1} + e^{i\mathbf{q}\cdot\mathbf{n}_2})/4$. The dispersion of the Majorana fermion is $2|s_{\mathbf{q}}|$, so $I(\omega)$ reflects density of states $g(\omega/2)$. The lower cutoff frequency of $I(\omega)$ measures the bulk gap 2Δ [Figs. 3(b) and 3(d)]. For the topological phase with Zeeman field, we find again $I(\omega) \propto g(\omega/2)$ with a modified factor [71], detecting the bulk topological gap, as plotted in Fig. 3(c).

Detection of chiral edge modes. The gapped Kitaev QSL hosts chiral Majorana edge modes, which emerge in the natural boundaries of the Rydberg atom array, and are a direct measurement of this exotic topological order. The high tunability of the present Rydberg platform enables unique schemes for the observation. We propose below two innovative detection strategies to identify and characterize the Majorana chiral edge modes.

The first strategy is to directly image the chiral motion of the Majorana edge modes. We show that the unidirectional quasiparticle flow of chiral edge states and the isotropic flow of the bulk states can be identified by examining merely the spin correlation dynamics. As illustrated in the inset of Figs. 4(a) and 4(b), we apply a pulse locally to suddenly tune $J_x \to J_x + \delta J_x$ on a specific x bond. The pulse couples to $s_i^x s_{j\langle ij\rangle_x}^x = -ic_i c_j/4$ and locally excites a two-particle wavepacket. We set the pulse strength as $\delta J_x = 0.5 J_x$ and the pulse duration as $\delta t = 0.1 J_x^{-1}$. The pulse consists of various frequencies, and Majorana fermions can be excited within a range of energy bands, and then move according to local band dispersion. Subsequently, we measure the motion via spin-correlation on the x bond, denoted as $\langle s_i^x(t) s_j^x(t)\rangle_{\langle ij\rangle_x}$, in two opposite directions indicated by blue arrows in Fig. 4. When the pulse is applied exclusively to the edge [Fig. 4(a)], the excited spin correlation evolves unidirectionally along the edge, implying an inherent consequence of the chiral nature of edge states, with group velocity given by the edge energy spectrum. In contrast, if the pulse is applied within the bulk, the spin correlation rapidly diffuses symmetrically throughout the entire system in Fig. 4(b). This sharp contrast provides a clear signature of the chiral Majorana modes in the topological QSL phase.

The second strategy is that we extend the light Bragg scattering technique for detecting Dirac fermion edge modes [75–78] to the present chiral Majorana edge modes in correlated spin liquid phase. Shining two lasers with wave vectors $\mathbf{k}_1(\omega_1)$ and $\mathbf{k}_2(\omega_2)$ on one row of the lattice [see the inset of Fig. 4(d)] induces a two-photon process characterized by $\Delta H'(\mathbf{q}) = \sum_{\langle ij\rangle_x} \Delta J' e^{i\mathbf{q}\cdot\mathbf{r}} s_i^x s_j^x$. Here $\boldsymbol{q} = \boldsymbol{k}_1 - \boldsymbol{k}_2 = q\hat{e}_x$ due to momentum conservation along the x direction. We obtain the dynamical structure factor $S(q, \omega)$ [71] for the scattering induced by the shinning lasers. Figures 4(c) and 4(d) depict the numerical simulation. When the perturbation is applied at the $y = 0$ edge, two groups of peaks are observed in Fig. 4(c), with one group located at lower frequencies, magnified in the inset, and the other group at higher frequencies. The low-frequency peaks exhibit the relationship $\omega = +qv_f$ when $q > 0$, arising from the transition between edge states. In comparison, the high-frequency peaks originate from the transition from bulk states around the smeared van Hove singularity at $k_x = \pi$ to edge states, and all show clearly the chirality of the edge modes. For $q < 0$, no resonant peak is observed since such edge states are all occupied [71]. The dynamical structure factors for shinning the bulk shows only finite frequency and symmetric peaks [Fig. 4(d)], implying that the bulk is gapped and nonchiral, in stark contrast to Majorana edge states.

Conclusion and outlook. We have proposed to realize and detect the Kitaev non-Abelian spin liquid in a deformed honeycomb array of Rydberg atoms with feasibility. A new LADDI mechanism is introduced to generate hopping and pairing terms in the hard-core boson representation, yielding the Kitaev exchange interactions in the x and y bonds. Together with engineering the van der Waals interactions, we realized a nearly pure Kitaev model with high precision. The gapped non-Abelian spin liquid phase with Ising-type anyons is further realized. Finally, based on measuring spin observables and the dynamical response, we proposed two innovative detection schemes to identify the gapless and chiral Majorana edge modes. This work opens up an avenue for analogy quantum simulation of exotic topological orders using Rydberg atoms. In particular, our original scheme for realizing the highly tunable exchange couplings not only facilitates the realization of Kitaev spin liquids, but also uncovers a

new pathway for the quantum simulation of a broad range of quantum spin models, with which the various exotic strongly correlated phases can be explored.

Acknowledgments. This work was supported by the National Key Research and Development Program of China (Grants No. 2021YFA1400900 and No. 2022YFA1405301), the National Natural Science Foundation of China (Grants No. 11825401, No. 12261160368, No. 11974421, and No. 12134020), the Innovation Program for Quantum Science and Technology (Grant No. 2021ZD0302000), and the Strategic Priority Research Program of the Chinese Academy of Science (Grant No. XDB28000000).

[1] X.-G. Wen, Colloquium: Zoo of quantum-topological phases of matter, Rev. Mod. Phys. **89**, 041004 (2017).

[2] A. Kitaev, Anyons in an exactly solved model and beyond, Ann. Phys. (NY) **321**, 2 (2006).

[3] C. Nayak, S. H. Simon, A. Stern, M. Freedman, and S. D. Sarma, Non-Abelian anyons and topological quantum computation, Rev. Mod. Phys. **80**, 1083 (2008).

[4] F. Wilczek, *Fractional Statistics and Anyon Superconductivity* (World Scientific, Singapore, 1990), Vol. 5.

[5] A. Stern, Non-Abelian states of matter, Nature (London) **464**, 187 (2010).

[6] G. Moore and N. Read, Nonabelions in the fractional quantum Hall effect, Nucl. Phys. B **360**, 362 (1991).

[7] X.-G. Wen, Non-Abelian statistics in the fractional quantum Hall states, Phys. Rev. Lett. **66**, 802 (1991).

[8] A. Y. Kitaev, Fault-tolerant quantum computation by anyons, Ann. Phys. (NY) **303**, 2 (2003).

[9] J. K. Pachos, *Introduction to Topological Quantum Computation* (Cambridge University Press, Cambridge, England, 2012).

[10] A. Stern and N. H. Lindner, Topological quantum computation–from basic concepts to first experiments, Science **339**, 1179 (2013).

[11] M. Hermanns, I. Kimchi, and J. Knolle, Physics of the Kitaev model: Fractionalization, dynamic correlations, and material connections, Annu. Rev. Condens. Matter Phys. **9**, 17 (2018).

[12] J. Knolle and R. Moessner, A field guide to spin liquids, Annu. Rev. Condens. Matter Phys. **10**, 451 (2019).

[13] H. Takagi, T. Takayama, G. Jackeli, G. Khaliullin, and S. E. Nagler, Concept and realization of Kitaev quantum spin liquids, Nat. Rev. Phys. **1**, 264 (2019).

[14] S. Trebst and C. Hickey, Kitaev materials, Phys. Rep. **950**, 1 (2022).

[15] A. Banerjee, J. Yan, J. Knolle, C. A. Bridges, M. B. Stone, M. D. Lumsden, D. G. Mandrus, D. A. Tennant, R. Moessner, and S. E. Nagler, Neutron scattering in the proximate quantum spin liquid α-$RuCl_3$, Science **356**, 1055 (2017).

[16] S.-H. Do, S.-Y. Park, J. Yoshitake, J. Nasu, Y. Motome, Y. S. Kwon, D. Adroja, D. Voneshen, K. Kim, T.-H. Jang *et al.*, Majorana fermions in the Kitaev quantum spin system α-$RuCl_3$, Nat. Phys. **13**, 1079 (2017).

[17] Y. Kasahara, T. Ohnishi, Y. Mizukami, O. Tanaka, S. Ma, K. Sugii, N. Kurita, H. Tanaka, J. Nasu, Y. Motome *et al.*, Majorana quantization and half-integer thermal quantum Hall effect in a Kitaev spin liquid, Nature (London) **559**, 227 (2018).

[18] T. Yokoi, S. Ma, Y. Kasahara, S. Kasahara, T. Shibauchi, N. Kurita, H. Tanaka, J. Nasu, Y. Motome, C. Hickey *et al.*, Half-integer quantized anomalous thermal Hall effect in the Kitaev material candidate α-$RuCl_3$, Science **373**, 568 (2021).

[19] J. Bruin, R. Claus, Y. Matsumoto, N. Kurita, H. Tanaka, and H. Takagi, Robustness of the thermal Hall effect close to half-quantization in α-$RuCl_3$, Nat. Phys. **18**, 401 (2022).

[20] S.-H. Baek, S.-H. Do, K.-Y. Choi, Y. S. Kwon, A.U.B. Wolter, S. Nishimoto, J. van Den Brink, and B. Büchner, Evidence for a field-induced quantum spin liquid in α-$RuCl_3$, Phys. Rev. Lett. **119**, 037201 (2017).

[21] R. Hentrich, A. U. Wolter, X. Zotos, W. Brenig, D. Nowak, A. Isaeva, T. Doert, A. Banerjee, P. Lampen-Kelley, D. G. Mandrus *et al.*, Unusual phonon heat transport in α-$RuCl_3$: strong spin-phonon scattering and field-induced spin gap, Phys. Rev. Lett. **120**, 117204 (2018).

[22] S. Bachus, D. A. S. Kaib, Y. Tokiwa, A. Jesche, V. Tsurkan, A. Loidl, S. M. Winter, A. A. Tsirlin, R. Valenti, and P. Gegenwart, Thermodynamic perspective on field-induced behavior of α-$RuCl_3$, Phys. Rev. Lett. **125**, 097203 (2020).

[23] I. A. Leahy, C. A. Pocs, P. E. Siegfried, D. Graf, S.-H. Do, K.-Y. Choi, B. Normand, and M. Lee, Anomalous thermal conductivity and magnetic torque response in the honeycomb magnet α-$RuCl_3$, Phys. Rev. Lett. **118**, 187203 (2017).

[24] N. Janša, A. Zorko, M. Gomilšek, M. Pregelj, K. W. Krämer, D. Biner, A. Biffin, C. Rüegg, and M. Klanjšek, Observation of two types of fractional excitation in the Kitaev honeycomb magnet, Nat. Phys. **14**, 786 (2018).

[25] S. M. Winter, K. Riedl, D. Kaib, R. Coldea, and R. Valentí, Probing α-$RuCl_3$ beyond magnetic order: Effects of temperature and magnetic field, Phys. Rev. Lett. **120**, 077203 (2018).

[26] L. E. Chern, E. Z. Zhang, and Y. B. Kim, Sign structure of thermal Hall conductivity and topological magnons for in-plane field polarized Kitaev magnets, Phys. Rev. Lett. **126**, 147201 (2021).

[27] I. M. Georgescu, S. Ashhab, and F. Nori, Quantum simulation, Rev. Mod. Phys. **86**, 153 (2014).

[28] A. J. Daley, I. Bloch, C. Kokail, S. Flannigan, N. Pearson, M. Troyer, and P. Zoller, Practical quantum advantage in quantum simulation, Nature (London) **607**, 667 (2022).

[29] L.-M. Duan, E. Demler, and M. D. Lukin, Controlling spin exchange interactions of ultracold atoms in optical lattices, Phys. Rev. Lett. **91**, 090402 (2003).

[30] A. D. Bookatz, P. Wocjan, and L. Viola, Hamiltonian quantum simulation with bounded-strength controls, New J. Phys. **16**, 045021 (2014).

[31] H. C. Po, L. Fidkowski, A. Vishwanath, and A. C. Potter, Radical chiral floquet phases in a periodically driven Kitaev model and beyond, Phys. Rev. B **96**, 245116 (2017).

[32] M. Kalinowski, N. Maskara, and M. D. Lukin, Non-Abelian floquet spin liquids in a digital Rydberg simulator, Phys. Rev. X **13**, 031008 (2023).

[33] B.-Y. Sun, N. Goldman, M. Aidelsburger, and M. Bukov, Engineering and probing non-Abelian chiral spin liquids using periodically driven ultracold atoms, PRX Quantum **4**, 020329 (2023).

[34] A. Browaeys and T. Lahaye, Many-body physics with individually controlled Rydberg atoms, Nat. Phys. **16**, 132 (2020).

[35] A. W. Glaetzle, M. Dalmonte, R. Nath, I. Rousochatzakis, R. Moessner, and P. Zoller, Quantum spin-ice and Dimer models with Rydberg atoms, Phys. Rev. X **4**, 041037 (2014).

[36] T. L. Nguyen, J.-M. Raimond, C. Sayrin, R. Cortinas, T. Cantat-Moltrecht, F. Assemat, I. Dotsenko, S. Gleyzes, S. Haroche, G. Roux *et al.*, Towards quantum simulation with circular Rydberg atoms, Phys. Rev. X **8**, 011032 (2018).

[37] A. Celi, B. Vermersch, O. Viyuela, H. Pichler, M. D. Lukin, and P. Zoller, Emerging two-dimensional gauge theories in Rydberg configurable arrays, Phys. Rev. X **10**, 021057 (2020).

[38] P. P. Mazza, R. Schmidt, and I. Lesanovsky, Vibrational dressing in kinetically constrained Rydberg spin systems, Phys. Rev. Lett. **125**, 033602 (2020).

[39] J. Y. Lee, J. Ramette, M. A. Metlitski, V. Vuletić, W. W. Ho, and S. Choi, Landau-forbidden quantum criticality in Rydberg quantum simulators, Phys. Rev. Lett. **131**, 083601 (2023).

[40] N. Nishad, A. Keselman, T. Lahaye, A. Browaeys, and S. Tsesses, Quantum simulation of generic spin-exchange models in Floquet-engineered Rydberg-atom arrays, Phys. Rev. A **108**, 053318 (2023).

[41] M. Kunimi, T. Tomita, H. Katsura, and Y. Kato, Proposal for simulating quantum spin models with the Dzyaloshinskii-Moriya interaction using Rydberg atoms and the construction of asymptotic quantum many-body scar states, Phys. Rev. A **110**, 043312 (2024).

[42] D. Barredo, S. De Léséleuc, V. Lienhard, T. Lahaye, and A. Browaeys, An atom-by-atom assembler of defect-free arbitrary two-dimensional atomic arrays, Science **354**, 1021 (2016).

[43] M. Endres, H. Bernien, A. Keesling, H. Levine, E. R. Anschuetz, A. Krajenbrink, C. Senko, V. Vuletic, M. Greiner, and M. D. Lukin, Atom-by-atom assembly of defect-free one-dimensional cold atom arrays, Science **354**, 1024 (2016).

[44] H. Kim, W. Lee, H.-g. Lee, H. Jo, Y. Song, and J. Ahn, *In situ* single-atom array synthesis using dynamic holographic optical tweezers, Nat. Commun. **7**, 13317 (2016).

[45] D. Barredo, V. Lienhard, S. De Leseleuc, T. Lahaye, and A. Browaeys, Synthetic three-dimensional atomic structures assembled atom by atom, Nature (London) **561**, 79 (2018).

[46] D. O. De Mello, D. Schäffner, J. Werkmann, T. Preuschoff, L. Kohfahl, M. Schlosser, and G. Birkl, Defect-free assembly of 2D clusters of more than 100 single-atom quantum systems, Phys. Rev. Lett. **122**, 203601 (2019).

[47] M. Saffman, T. G. Walker, and K. Mølmer, Quantum information with Rydberg atoms, Rev. Mod. Phys. **82**, 2313 (2010).

[48] H. Labuhn, D. Barredo, S. Ravets, S. De Léséleuc, T. Macrì, T. Lahaye, and A. Browaeys, Tunable two-dimensional arrays of single Rydberg atoms for realizing quantum Ising models, Nature (London) **534**, 667 (2016).

[49] H. Bernien, S. Schwartz, A. Keesling, H. Levine, A. Omran, H. Pichler, S. Choi, A. S. Zibrov, M. Endres, M. Greiner *et al.*, Probing many-body dynamics on a 51-atom quantum simulator, Nature (London) **551**, 579 (2017).

[50] A. Keesling, A. Omran, H. Levine, H. Bernien, H. Pichler, S. Choi, R. Samajdar, S. Schwartz, P. Silvi, S. Sachdev *et al.*, Quantum Kibble–Zurek mechanism and critical dynamics on a programmable Rydberg simulator, Nature (London) **568**, 207 (2019).

[51] P. Scholl, M. Schuler, H. J. Williams, A. A. Eberharter, D. Barredo, K.-N. Schymik, V. Lienhard, L.-P. Henry, T. C. Lang, T. Lahaye *et al.*, Quantum simulation of 2D antiferromagnets with hundreds of Rydberg atoms, Nature (London) **595**, 233 (2021).

[52] S. Ebadi, T. T. Wang, H. Levine, A. Keesling, G. Semeghini, A. Omran, D. Bluvstein, R. Samajdar, H. Pichler, W. W. Ho *et al.*, Quantum phases of matter on a 256-atom programmable quantum simulator, Nature (London) **595**, 227 (2021).

[53] D. Bluvstein, A. Omran, H. Levine, A. Keesling, G. Semeghini, S. Ebadi, T. T. Wang, A. A. Michailidis, N. Maskara, W. W. Ho *et al.*, Controlling quantum many-body dynamics in driven Rydberg atom arrays, Science **371**, 1355 (2021).

[54] D. Barredo, H. Labuhn, S. Ravets, T. Lahaye, A. Browaeys, and C. S. Adams, Coherent excitation transfer in a spin chain of three Rydberg atoms, Phys. Rev. Lett. **114**, 113002 (2015).

[55] C. Chen, G. Bornet, M. Bintz, G. Emperauger, L. Leclerc, V. S. Liu, P. Scholl, D. Barredo, J. Hauschild, S. Chatterjee *et al.*, Continuous symmetry breaking in a two-dimensional Rydberg array, Nature (London) **616**, 691 (2023).

[56] S. de Léséleuc, V. Lienhard, P. Scholl, D. Barredo, S. Weber, N. Lang, H. P. Büchler, T. Lahaye, and A. Browaeys, Observation of a symmetry-protected topological phase of interacting bosons with Rydberg atoms, Science **365**, 775 (2019).

[57] G. Semeghini, H. Levine, A. Keesling, S. Ebadi, T. T. Wang, D. Bluvstein, R. Verresen, H. Pichler, M. Kalinowski, R. Samajdar *et al.*, Probing topological spin liquids on a programmable quantum simulator, Science **374**, 1242 (2021).

[58] T.-H. Yang, B.-Z. Wang, X.-C. Zhou, and X.-J. Liu, Quantum Hall states for Rydberg arrays with laser-assisted dipole-dipole interactions, Phys. Rev. A **106**, L021101 (2022).

[59] T. F. J. Poon, X.-C. Zhou, B.-Z. Wang, T.-H. Yang, and X.-J. Liu, Fractional quantum anomalous Hall phase for Raman superarray of Rydberg atoms, Adv. Quantum Technol. **7**, 2300356 (2024).

[60] X.-C. Zhou, Y. Wang, T.-F. J. Poon, Q. Zhou, and X.-J. Liu, Exact new mobility edges between critical and localized states, Phys. Rev. Lett. **131**, 176401 (2023).

[61] M. Aidelsburger, M. Atala, M. Lohse, J. T. Barreiro, B. Paredes, and I. Bloch, Realization of the Hofstadter hamiltonian with ultracold atoms in optical lattices, Phys. Rev. Lett. **111**, 185301 (2013).

[62] H. Miyake, G. A. Siviloglou, C. J. Kennedy, W. C. Burton, and W. Ketterle, Realizing the Harper Hamiltonian with laser-assisted tunneling in optical lattices, Phys. Rev. Lett. **111**, 185302 (2013).

[63] X.-J. Liu, K. T. Law, and T. K. Ng, Realization of 2D spin-orbit interaction and exotic topological orders in cold atoms, Phys. Rev. Lett. **112**, 086401 (2014).

[64] M. Aidelsburger, M. Lohse, C. Schweizer, M. Atala, J. T. Barreiro, S. Nascimbène, N. Cooper, I. Bloch, and N. Goldman, Measuring the Chern number of Hofstadter bands with ultracold bosonic atoms, Nat. Phys. **11**, 162 (2015).

[65] Z. Wu, L. Zhang, W. Sun, X.-T. Xu, B.-Z. Wang, S.-C. Ji, Y. Deng, S. Chen, X.-J. Liu, and J.-W. Pan, Realization of two-dimensional spin-orbit coupling for Bose-Einstein condensates, Science **354**, 83 (2016).

[66] X.-J. Liu, Z.-X. Liu, K. T. Law, W. V. Liu, and T. K. Ng, Chiral topological orders in an optical Raman lattice, New J. Phys. **18**, 035004 (2016).

[67] B. Song, L. Zhang, C. He, T. F. J. Poon, E. Hajiyev, S. Zhang, X.-J. Liu, and G.-B. Jo, Observation of symmetry-protected topological band with ultracold fermions, Sci. Adv. **4**, eaao4748 (2018).

[68] Y.-H. Lu, B.-Z. Wang, and X.-J. Liu, Ideal Weyl semimetal with 3D spin-orbit coupled ultracold quantum gas, Sci. Bull. **65**, 2080 (2020).

[69] Z.-Y. Wang, X.-C. Cheng, B.-Z. Wang, J.-Y. Zhang, Y.-H. Lu, C.-R. Yi, S. Niu, Y. Deng, X.-J. Liu, S. Chen *et al.*, Realization of an ideal Weyl semimetal band in a quantum gas with 3D spin-orbit coupling, Science **372**, 271 (2021).

[70] J^{γ}_{+-} (J^{γ}_{--}) denote the hopping (pairing) term across the γ bond.

[71] See Supplemental Material at http://link.aps.org/supplemental/10.1103/PhysRevResearch.6.L042054 for about the laser assisted dipole-dipole interaction, numerical estimate of parameters, and the detection schemes, which includes Refs. [79–83].

[72] Z. Zhu, I. Kimchi, D. Sheng, and L. Fu, Robust non-Abelian spin liquid and a possible intermediate phase in the antiferromagnetic Kitaev model with magnetic field, Phys. Rev. B **97**, 241110 (2018).

[73] S. R. Cohen and J. D. Thompson, Quantum computing with circular Rydberg atoms, PRX Quantum **2**, 030322 (2021).

[74] J. Knolle, G.-W. Chern, D. Kovrizhin, R. Moessner, and N. Perkins, Raman scattering signatures of Kitaev spin liquids in A2IrO_3 iridates with A =Na or Li, Phys. Rev. Lett. **113**, 187201 (2014).

[75] X.-J. Liu, X. Liu, C. Wu, and J. Sinova, Quantum anomalous Hall effect with cold atoms trapped in a square lattice, Phys. Rev. A **81**, 033622 (2010).

[76] T. D. Stanescu, V. Galitski, and S. D. Sarma, Topological states in two-dimensional optical lattices, Phys. Rev. A **82**, 013608 (2010).

[77] N. Goldman, J. Beugnon, and F. Gerbier, Detecting chiral edge states in the Hofstadter optical lattice, Phys. Rev. Lett. **108**, 255303 (2012).

[78] M. Buchhold, D. Cocks, and W. Hofstetter, Effects of smooth boundaries on topological edge modes in optical lattices, Phys. Rev. A **85**, 063614 (2012).

[79] T. G. Walker and M. Saffman, Consequences of Zeeman degeneracy for the van der Waals blockade between Rydberg atoms, Phys. Rev. A **77**, 032723 (2008).

[80] D. Barredo, V. Lienhard, P. Scholl, S. de Léséleuc, T. Boulier, A. Browaeys, and T. Lahaye, Three-dimensional trapping of individual Rydberg atoms in ponderomotive bottle beam traps, Phys. Rev. Lett. **124**, 023201 (2020).

[81] Y. Mei, Y. Li, H. Nguyen, P. Berman, and A. Kuzmich, Trapped alkali-metal Rydberg qubit, Phys. Rev. Lett. **128**, 123601 (2022).

[82] E. H. Lieb, Flux phase of the half-filled band, Phys. Rev. Lett. **73**, 2158 (1994).

[83] F. D. M. Haldane, Model for a quantum Hall effect without Landau levels: Condensed-matter realization of the "parity anomaly", Phys. Rev. Lett. **61**, 2015 (1988).